

Automatic Pixelwise Object Labeling for Aerial Imagery Using Stacked U-Nets

Andrew Khalel
Raisa Energy LLC
Faculty of Engineering, Cairo University
Cairo, Egypt
andrewekhalel@eng.cu.edu.eg

Motaz El-Saban
Raisa Energy LLC
Faculty of Computers and Information, Cairo University
Cairo, Egypt
melsaban@raisaenergy.com

Abstract—Automation of objects labeling in aerial imagery is a computer vision task with numerous practical applications. Fields like energy exploration require an automated method to process a continuous stream of imagery on a daily basis. In this paper we propose a pipeline to tackle this problem using a stack of convolutional neural networks (U-Net architecture) arranged end-to-end. Each network works as post-processor to the previous one. Our model outperforms current state-of-the-art on two different datasets: Inria Aerial Image Labeling dataset and Massachusetts Buildings dataset each with different characteristics such as spatial resolution, object shapes and scales. Moreover, we experimentally validate computation time savings by processing sub-sampled images and later upsampling pixelwise labeling. These savings come at a negligible degradation in segmentation quality. Though the conducted experiments in this paper cover only aerial imagery, the technique presented is general and can handle other types of images.

Keywords-Remote Sensing; Semantic Segmentation; U-Net; Object Labeling; Deep Convolutional Neural Networks

I. INTRODUCTION

Since the introduction of high spatial and temporal resolution aerial imagery services, aerial imagery became one of the most important components in various industries. Energy, mining, civil, defense and more industries are able to use aerial imagery to enhance their productivity and quality of work. One of the most costly and time consuming tasks needed for using aerial imagery is the labeling task. In addition, hand labeling for objects of interest requires domain expertise for perfect labeling.

Recent breakthroughs in image understanding techniques using deep learning approaches together with the leap in hardware technologies specifically GPUs opened the door for more researchers to experiment with different approaches and techniques. Deep learning approaches are now deployable in industry at an affordable cost.

Generally, object labeling can be approached in two ways: localization and segmentation. Localization is where a bounding box is drawn around the detected object. The problem in localization is that the bounding box is not actually representing object's borders and can't describe its shape. On the contrary, segmentation is labeling pixels/super pixels representing the object. This will result in a very

detailed detection for shape, size and outline of the object. Since objects of interest usually don't have a uniform or a fixed shape, we chose the segmentation approach for more accurate results.

This paper has two main contributions: First, we introduce a new DCNN semantic image segmentation architecture based on stacked U-nets where each network enhances the results of previous one. In our experiments on aerial imagery a cascade of two U-Nets was sufficient to outperform current state-of-the-art on two different datasets each with different characteristics. Secondly, We experiment the effect of image spatial resolution on our model performance. We find that downscaling of original resolution can decrease computation time significantly at the expense of a negligible loss in segmentation quality.

The next sections are organized as follows. Section 2 illustrates related work in the literature of semantic image segmentation. Section 3 details our methodology to approach a high quality segmentation. Section 4 presents different experiments and results to demonstrate the power of our methodology. Finally, paper conclusion and direction for future work are presented in section 5.

II. RELATED WORK

Semantic image segmentation is the process of partitioning the image into meaningful parts, each part belongs to one of the pre-specified classes. Approaches used for semantic segmentation can be divided into: traditional and deep learning approaches. Traditional approaches usually depend on domain knowledge to extract features and apply these features to techniques like: Texton Forests [1], Random Forests [2], [3], SVM [4], [5] and Conditional Random Fields (CRFs) [6].

One of the challenges semantic segmentation can help addressing is extracting objects of interest from the scene. The problem we are trying to address in this paper is to extract buildings from aerial imagery which has been attempted previously using different approaches. Many of these approaches use hand-crafted features, classifiers and boosting [7]–[9] or contour detection to find a rectangular (building-like) objects [10].

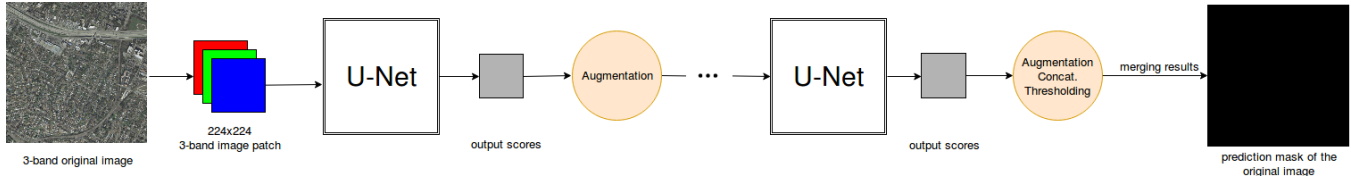


Figure 1: Full system pipeline overview

Li et al. [11] uses the unsupervised Gaussian mixture model (GMM) to segment the image into homogeneous super pixels and then Higher order Conditional Random Field (HCRF) is used for accurate rooftop extraction. Jin and Davis [12] generate building hypothesis using edge-based segmentation methods and verified them using differential morphological profile (DMP). Buildings are extracted using structural, contextual, and spectral information.

In recent years deep learning methods have shown excellent performance in many fields including semantic segmentation. Long et al. [13] introduced the Fully Connected Networks (FCN) as an end-to-end architecture producing dense output maps. Long also introduced the concept of upsampling using deconvolutional layers. Since object location is very important in semantic segmentation - unlike in classification - new architectures were developed to preserve this location information.

First set of architectures are inspired by the idea of encoder-decoder where the input image is encoded into smaller intermediate form using pooling layers and then recovered to original size using upsampling layers in the decoder usually with help of skip connections from encoder to decoder. Most popular architectures of this set are: (1) U-Net introduced by Ronneberger et al. [14] originally for medical image segmentation. U-Net won the ISBI cell tracking challenge 2015 with a large margin. (2) SegNet [15] which doesn't use skip connections and saves the pooling indices to be used in the decoder for non-linear upsampling.

A different set of architectures depends on atrous (also called dilated) convolution [16] instead of pooling layers. In atrous convolution filters are "with holes" so that we can enlarge the receptive field of the filter without decreasing the image spatial resolution.

Volodymyr Mnih uses convolutional neural networks in his PhD thesis [17] to train an aerial image labeling system for roads and buildings. He tried neural networks and Conditional Random Fields as post-processing to CNN. His model shows good performance on Massachusetts roads and buildings datasets [17].

Saito and Aoki [18] use CNN for road and building detection. They use the normal downsampling architecture of the CNN and at the end, a fully connected layer with Dropout [19] is added to infer prediction of the input image. Their model outperforms Mnih's models [17] for both roads and buildings using a single model for each class.

Newell et al. [20] propose a network architecture that reaches state-of-the-art results in human pose estimation. They call their architecture Hourglass due to its shape of contracting and expanding paths. This architecture is very similar to U-Net, it only differs in the way tensors are concatenated. Hourglass uses addition operator to add the two tensors together into a new sum tensor. Human pose estimation problem can be formulated as the task of extraction joints from an input image. With this formulation, we can adapt the same network architecture for the task of semantic image segmentation.

III. METHODOLOGY

An overview of our full pipeline is shown in Figure 1. Our pipeline starts by dividing the input image into smaller patches 224x224x3 pixels. These patches are the input of our model and the output is a cropped prediction mask. By concatenating these small outputs, we can get a full size prediction mask. More levels of U-Nets are used to enhance the results.

A. Network architecture

As shown in Figure 2 most of our layers consist of 3x3 convolution filters since they are computationally efficient. Filters' count double as we go deeper in the contracting path while they are halved while going through the expanding path. Each layer also has Batch Normalization [21] layer for faster convergence. Max pooling with size of 2x2 is used for down sampling while for up-sampling, elements in the original tensor are replicated to its 2x2 window in the output up-sampled tensor. Concatenation is done by appending the two tensors into a new activation volume. Finally, He uniform variance scaling initializer [22] is used for all convolutional layers.

The partitioning of the whole image into smaller patches will cause buildings on the patch edges to lose important parts of their structure which leads to poor performance at edges. This problem can be solved in two ways: using overlapped patches or using cropping layer in our network. We used cropping layer as it turns out to be more effective solution [23].

1) *Training*: Nadam optimizer [24] is used to train the model. For the first level U-Net a learning rate of 1e-3 is used for 50 epochs and then 1e-4 is used for another 50 epochs. A batch size of 128 patches is used. The second

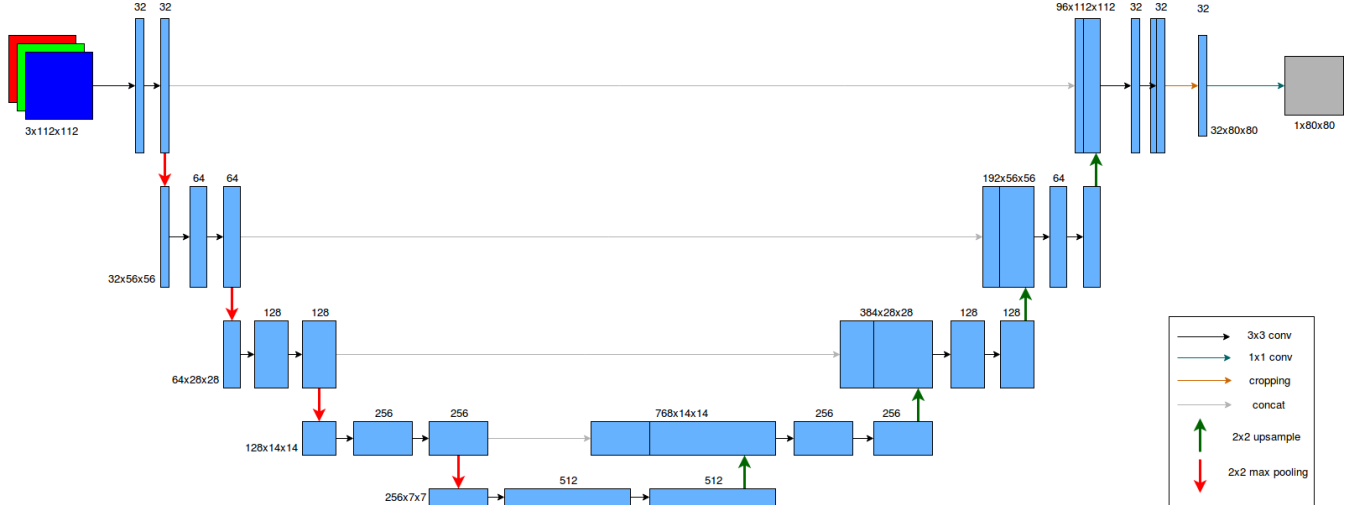


Figure 2: Detailed architecture of our U-Net

level U-Net uses a learning rate of $1e-4$ and is trained for 50 epochs. Since Intersection over Union (IoU) becomes the standard metric in semantic image segmentation [13] and it is non-differentiable, a joint loss function L proposed by Iglovikov et al. [23] is used to combine both a differentiable form of IoU and binary cross entropy

$$H = -\frac{1}{n} \sum_{i=1}^n [y \log(\hat{y}) + (1 - y) \log(1 - \hat{y})]$$

$$J(y, \hat{y}) = \frac{1}{n} \sum_{i=1}^n \frac{y_i \cdot \hat{y}_i}{y_i + y_i - \hat{y}_i \cdot \hat{y}_i}$$

$$L = H - \log(J)$$

where n is the number of images in a batch, y is the ground-truth value and \hat{y} is the prediction.

Moreover, data augmentation is applied at training time by choosing randomly from a set of transformations: horizontal flip, vertical flip and rotations. Data augmentation helps in building a strong model which is less dependent on input image orientation. This is very helpful for our model to generalize to different regions other than regions in training set.

2) *Prediction*: To make more confident predictions, test time augmentations are applied where the same set of transformation applied at training time is applied to each image patch before prediction. The predictions of all transformed versions are averaged. This average is the final prediction score. Then, thresholding is applied to convert scores into binary values of the mask. The threshold value is a hyperparameter which we tuned using cross validation set.

To reduce discontinuity effect of image sub-division into tiles we use image mirroring as proposed by Ron-

neberger et al. [14]. This yields better results at tile boundaries. Our pipeline is built using Keras [25] library with Theano [26] as backend.

IV. RESULTS

In this section we introduce the datasets used in experimentation and report on conducted experiments and their results.

A. Datasets

To illustrate the power of the proposed model we use two datasets: Inria Aerial Image Labeling dataset [27] and Massachusetts Buildings dataset [17]. We selected these two datasets because they cover different imagery characteristics such as spatial resolution, object types, shapes and sizes.

Inria's dataset is specifically constructed to address automatic pixelwise labeling of aerial imagery. The dataset consists of two subsets: training and testing sets. Each subset covers 405 km^2 area with spatial resolution of 0.3 m . The provided data are 3-band colored orthorectified images. Training data is labeled for two classes: building and not building. Training dataset covers Austin, Chicago, Kitsap County, Western Tyrol and Vienna, while test set covers a set of different regions: Bellingham, Bloomington, Innsbruck, San Francisco, Eastern Tyrol. For each region in the two subsets, there are 36 tiles of size 5000×5000 pixels that cover $1500 \times 1500 \text{ m}$ area. A sample from the dataset images and labels is shown in Figure 4.

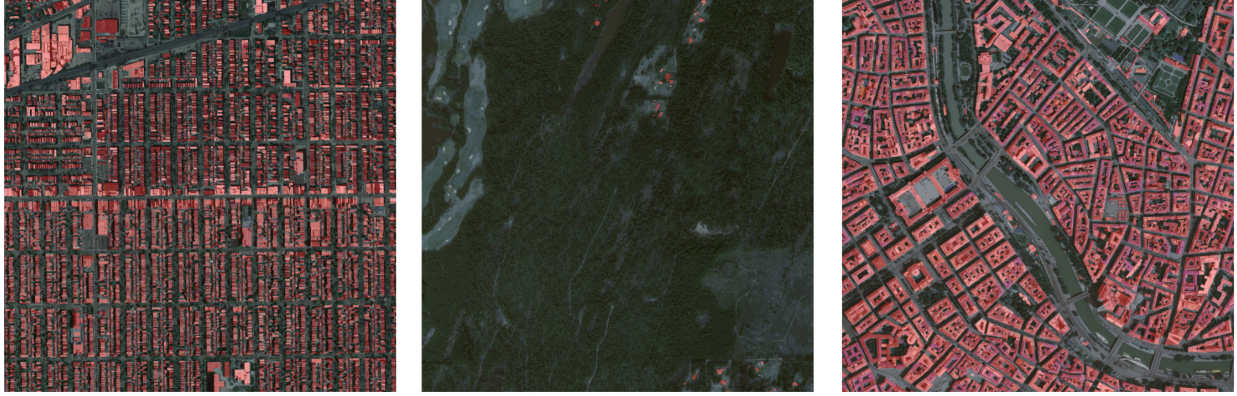


Figure 3: Different urban densities in the dataset. Chicago, Kitsap County, and Vienna respectively. Red areas represent buildings' ground truth labels



Figure 4: A sample of Inria's dataset from authors' website [28] aerial images (on the left) and buildings' ground truth mask (on the right)

There are two important aspects to choose Inria's dataset for our experiments. First, training and testing sets cover different regions so we will be able to judge the ability of our model to generalize to new regions. Secondly, the covered regions are very different in their urban densities. Figure 3 shows the large variety of urban densities in different regions. Chicago has very dense and small buildings. Kitsap county has a very sparse distribution of buildings due to its large green areas. Vienna has a very different architecture style: large buildings without a full roof. This variability in the dataset ensures that the model will learn to label different regions and understands the structure of a building in a more general sense.

The second dataset we use is the Massachusetts buildings dataset. It consists of 151 aerial images of size 1500x1500 pixels covering urban and suburban regions at the area of Boston. Each image covers an area of 2.25 km² at a resolution 1 m²/pixel. These images were randomly split into training, validation and test sets with sizes 137, 4 and 10 respectively. A sample of the dataset is shown at Figure 5.

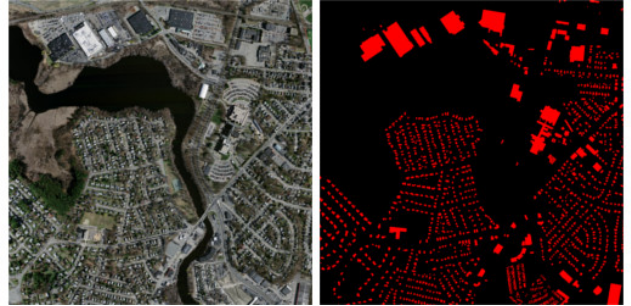


Figure 5: A sample of Massachusetts buildings dataset with aerial image and buildings' mask.

In order to enable comparison with results from other researchers, we use the same performance measures of each dataset. Inria's dataset uses two main performance measures which are: Intersection over Union (IoU) and Accuracy. Intersection over union, also known as Jaccard index is defined as:

$$IoU(GT, P) = \frac{\text{Area of Intersection between GT and P}}{\text{Area of Union between GT and P}}$$

where GT is the ground truth mask and P is the predicted mask. Accuracy is defined as:

$$Accuracy(GT, P) = \frac{\text{Area of correctly classified pixels}}{\text{Area of GT}}$$

We focused our experiments on IoU as it becomes a standard for semantic segmentation [13]. Moreover, accuracy is not discriminative enough since large image areas are dedicated to background (non-building) class.

For Massachusetts buildings dataset, a relaxed version of precision and recall is used to calculate the precision-recall breakeven point [17]. The relaxation assumption is to consider a positive label correct if it falls within the 7x7 region of any ground truth positive pixel. Since the buildings' masks are usually not perfectly aligned to the image, this relaxation will provide a realistic performance measure.

B. Best model results

After running through all experiments and choosing the best model described in section III, We compare our results with the results of other approaches as shown in table I. Figure 6 shows the resulting labels of our model on an image of Innsbruck from the test set. The figure shows detections of buildings with different shapes (rectangular and non-rectangular) and sizes.



Figure 6: Our model labels (red) for buildings with different shapes at Innsbruck

In some cases our model computes a wrong segmentation result. For example in figure 7 we can see the model detecting a parking lot as a building due to its color which is very similar to buildings colors in this area and due to its texture which looks like house's roof.

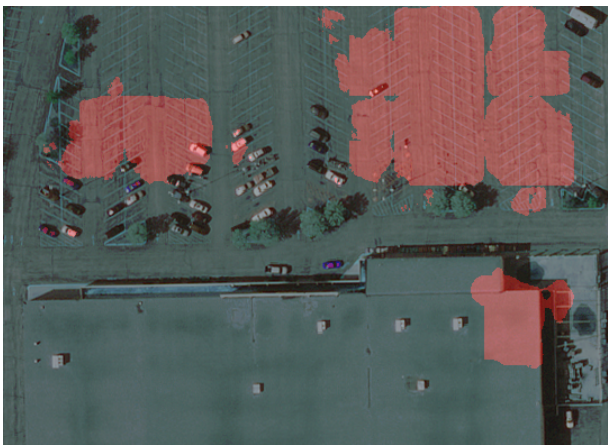


Figure 7: False positives at Bloomington

Table II shows our model results on the Massachusetts building dataset. We significantly outperform other approaches from the literature. Figure 8 shows a sample of our model predictions. Although the two datasets' characteristics are quite different our model has leading results on both of them with the same architecture.



Figure 8: Our model labels (red) for buildings on Massachusetts dataset

The training time of the first U-Net was 41 hours on Nvidia Tesla K80 GPU, while for the second U-Net, training time was 20.8 hours. Prediction of a single tile of size (5000x500 pixels) took 3.48 minutes including the augmentation, concatenating small patches and thresholding.

C. Different architectures and pipelines

After presenting our model best results, we present in this section several variations we have experimented with. The goal is to highlight key factors leading to the superior performance of our model. Table III shows results for different conducted experiments on Inria's dataset. Using a single U-Net architecture to directly predict the image is a good starting point. Since data augmentation is very important to produce a robust model which is invariant to different rotations and orientations, we test its effect on the results by running the same model of a single U-Net with the same configurations in addition to the augmentation on both training and testing time. This change leads to an enhancement in IoU of the validation set as shown in the results.

Applying Hourglass [20] architecture with data augmentation to our problem gives an IoU score of 72.30. Although Hourglass didn't produce better results, it guided us to the idea of networks stacking (our final pipeline). Stacked Hourglass architecture consists of multiple consecutive Hourglasses arranged end-to-end.

D. Downsampling

As mentioned before the spatial resolution of Inria's dataset is 0.3 m. We want to investigate the effect of lower resolution on the results. To try different resolutions of the same data, we re-sample the data at lower rates. Our experiments are conducted at two resolutions: $\frac{1}{2}$ and $\frac{1}{4}$ the original resolution. To ensure fair comparison between different resolutions, we upsample the lower resolution masks to the original resolution after the prediction using simple linear interpolation before calculating Jaccard index. The result of

Method		Austin	Chicago	Kitsap Co.	West Tyrol	Vienna	Overall
FCN + MLP [27] (Baseline)	IoU	61.20	61.30	51.50	57.95	72.13	64.67
	Acc.	94.20	90.43	98.92	96.66	91.87	94.42
SegNet (Single-Loss) [29]	IoU	76.49	66.77	72.69	66.35	76.25	72.57
	Acc.	93.12	99.24	97.79	91.58	96.55	95.66
SegNet + MultiTask-Loss [29] (Uncertainty Weighted)	IoU	76.76	67.06	73.30	66.91	76.68	73.00
	Acc.	93.21	99.25	97.84	91.71	96.61	95.73
2-levels U-Nets + aug. (Our model)	IoU	77.29	68.52	72.84	75.38	78.72	74.55
	Acc.	96.69	92.40	99.25	98.11	93.79	96.05

Table I: Results of different methods for Inria Aerial Image Labeling validation set

Method	Precision-recall breakevent point
Mnih et al. [17]	0.9211
Saito et al. [18]	0.9230
Marcu et al. [30]	0.9423
Our model	0.9633

Table II: Precision-recall breakeven point of different approaches for the Massachusetts dataset.

Method	IoU
Single U-Net	73.68
Single U-Net + aug.	74.38
Single U-Net + aug. + CRF	72.58
Single Hourglass + aug.	72.30
2-level U-Nets + aug.	74.60

Table III: IoU of different pipelines for Inria Aerial Image Labeling dataset.

our single U-Net model with only 50 epochs of training on different resolutions is shown in Table IV along with the prediction time per image. As the table illustrates, the results

Resolution	IoU	Prediction time (secs/tile)
1	71.23	~160
1/2	71.07	~40
1/4	70.71	~17

Table IV: IoU and prediction time per full image (tile) at different resolutions using a single U-Net architecture.

for lower resolutions are very close to the results of the original resolution. However, there are substantial savings in prediction time. Also, the overhead of downsampling and upsampling is negligible (~0.06 secs/image). These findings show that a very high resolution can be replaced by a lower one for considerable gains in computation time.

E. Using Conditional Random Fields (CRFs) [31] as post-processing

Fully connected CRFs proved to be very effective for the localization challenge [16], [32]. They are capable of finding fine-grained edges and outlines which enhances object segmentation quality.



Figure 9: detected building after CRF processing. The real satellite image is on the left while the detected mask is on the right

Using CRF with a single U-Net scored 72.58 on the validation set. Figure 9 shows clearly how CRF draws detailed outer and inner edges of the detected building however this isn't required for our datasets. Our datasets requires a solid polygon covering the whole building without any roof details and lines. Based on these results we have not incorporated CRFs as post-processor to our pipeline.

V. CONCLUSION AND FUTURE WORK

In this paper we propose a stack of deep convolutional neural networks built on the U-Net [14] architecture to perform pixelwise labeling of aerial images. Our approach outperforms all other models on both Inria's aerial image labeling dataset [27] and Massachusetts Buildings dataset [17]. In addition, experiments show that we can achieve sizable gains in processing time by working on lower resolution images. This could be very helpful for interactive applications that require fast labeling.

For future work, we will investigate suitable methods that can adapt learned models at one specific spatial resolution to work on different resolutions with minimal changes as this can be very useful for models to learn on a dataset starting from a model trained on a different dataset. Another possible future direction is to leverage Generative Adversarial Networks (GANs) [33] to improve model segmentation quality through a generator-discriminator network pair.

REFERENCES

- [1] J. Shotton, M. Johnson, and R. Cipolla, "Semantic texton forests for image categorization and segmentation," in *Computer vision and pattern recognition, 2008. CVPR 2008. IEEE Conference on*. IEEE, 2008, pp. 1–8.

- [2] J. Shotton, T. Sharp, A. Kipman, A. Fitzgibbon, M. Finocchio, A. Blake, M. Cook, and R. Moore, "Real-time human pose recognition in parts from single depth images," *Communications of the ACM*, vol. 56, no. 1, pp. 116–124, 2013.
- [3] F. Schroff, A. Criminisi, and A. Zisserman, "Object class segmentation using random forests." in *BMVC*, 2008, pp. 1–10.
- [4] Y. Yang, S. Hallman, D. Ramanan, and C. C. Fowlkes, "Layered object models for image segmentation," *IEEE Transactions on Pattern Analysis and Machine Intelligence*, vol. 34, no. 9, pp. 1731–1743, 2012.
- [5] P. F. Felzenszwalb, R. B. Girshick, D. McAllester, and D. Ramanan, "Object detection with discriminatively trained part-based models," *IEEE transactions on pattern analysis and machine intelligence*, vol. 32, no. 9, pp. 1627–1645, 2010.
- [6] C. Russell, P. Kohli, P. H. Torr *et al.*, "Associative hierarchical crfs for object class image segmentation," in *Computer Vision, 2009 IEEE 12th International Conference on*. IEEE, 2009, pp. 739–746.
- [7] J. Inglada, "Automatic recognition of man-made objects in high resolution optical remote sensing images by svm classification of geometric image features," *ISPRS journal of photogrammetry and remote sensing*, vol. 62, no. 3, pp. 236–248, 2007.
- [8] J. Porway, K. Wang, B. Yao, and S. C. Zhu, "A hierarchical and contextual model for aerial image understanding," in *Computer Vision and Pattern Recognition, 2008. CVPR 2008. IEEE Conference on*. IEEE, 2008, pp. 1–8.
- [9] C. Senaras, M. Ozay, and F. T. Y. Vural, "Building detection with decision fusion," *IEEE journal of selected topics in applied earth observations and remote sensing*, vol. 6, no. 3, pp. 1295–1304, 2013.
- [10] T. Kim and J.-P. Muller, "Development of a graph-based approach for building detection," *Image and Vision Computing*, vol. 17, no. 1, pp. 3–14, 1999.
- [11] E. Li, J. Femiani, S. Xu, X. Zhang, and P. Wonka, "Robust rooftop extraction from visible band images using higher order crf," *IEEE Transactions on Geoscience and Remote Sensing*, vol. 53, no. 8, pp. 4483–4495, 2015.
- [12] X. Jin and C. H. Davis, "Automated building extraction from high-resolution satellite imagery in urban areas using structural, contextual, and spectral information," *EURASIP Journal on Advances in Signal Processing*, vol. 2005, no. 14, p. 745309, 2005.
- [13] J. Long, E. Shelhamer, and T. Darrell, "Fully convolutional networks for semantic segmentation," in *Proceedings of the IEEE Conference on Computer Vision and Pattern Recognition*, 2015, pp. 3431–3440.
- [14] O. Ronneberger, P. Fischer, and T. Brox, "U-net: Convolutional networks for biomedical image segmentation," in *International Conference on Medical Image Computing and Computer-Assisted Intervention*. Springer, 2015, pp. 234–241.
- [15] V. Badrinarayanan, A. Kendall, and R. Cipolla, "Segnet: A deep convolutional encoder-decoder architecture for image segmentation," *arXiv preprint arXiv:1511.00561*, 2015.
- [16] L.-C. Chen, G. Papandreou, I. Kokkinos, K. Murphy, and A. L. Yuille, "Deeplab: Semantic image segmentation with deep convolutional nets, atrous convolution, and fully connected crfs," *arXiv preprint arXiv:1606.00915*, 2016.
- [17] V. Mnih, "Machine learning for aerial image labeling," Ph.D. dissertation, University of Toronto, 2013.
- [18] S. Saito and Y. Aoki, "Building and road detection from large aerial imagery," in *SPIE/IS&T Electronic Imaging*. International Society for Optics and Photonics, 2015, pp. 94 050K–94 050K.
- [19] N. Srivastava, G. E. Hinton, A. Krizhevsky, I. Sutskever, and R. Salakhutdinov, "Dropout: a simple way to prevent neural networks from overfitting," *Journal of machine learning research*, vol. 15, no. 1, pp. 1929–1958, 2014.
- [20] A. Newell, K. Yang, and J. Deng, "Stacked hourglass networks for human pose estimation," in *European Conference on Computer Vision*. Springer, 2016, pp. 483–499.
- [21] S. Ioffe and C. Szegedy, "Batch normalization: Accelerating deep network training by reducing internal covariate shift," in *International Conference on Machine Learning*, 2015, pp. 448–456.
- [22] K. He, X. Zhang, S. Ren, and J. Sun, "Delving deep into rectifiers: Surpassing human-level performance on imagenet classification," in *Proceedings of the IEEE international conference on computer vision*, 2015, pp. 1026–1034.
- [23] V. Iglovikov, S. Mushinskiy, and V. Osin, "Satellite imagery feature detection using deep convolutional neural network: A kaggle competition," *arXiv preprint arXiv:1706.06169*, 2017.
- [24] T. Dozat, "Incorporating nesterov momentum into adam," 2016.
- [25] F. Chollet *et al.*, "Keras," <https://github.com/fchollet/keras>, 2015.
- [26] Theano Development Team, "Theano: A Python framework for fast computation of mathematical expressions," *arXiv e-prints*, vol. abs/1605.02688, May 2016. [Online]. Available: <http://arxiv.org/abs/1605.02688>
- [27] E. Maggiori, Y. Tarabalka, G. Charpiat, and P. Alliez, "Can semantic labeling methods generalize to any city? the inria aerial image labeling benchmark," in *IEEE International Geoscience and Remote Sensing Symposium (IGARSS)*. IEEE, 2017.
- [28] Inria, "Inria Aerial Image Labeling Dataset," <https://project.inria.fr/aerialimagelabeling/>, 2017, [Online; accessed 6-September-2017].
- [29] B. Bischke, P. Helber, J. Folz, D. Borth, and A. Dengel, "Multi-task learning for segmentation of building footprints with deep neural networks," *arXiv preprint arXiv:1709.05932*, 2017.

- [30] A. E. Marcu, "A local-global approach to semantic segmentation in aerial images," *arXiv preprint arXiv:1607.05620*, 2016.
- [31] J. Lafferty, A. McCallum, and F. C. Pereira, "Conditional random fields: Probabilistic models for segmenting and labeling sequence data," 2001.
- [32] P. Krähenbühl and V. Koltun, "Efficient inference in fully connected crfs with gaussian edge potentials," in *Advances in neural information processing systems*, 2011, pp. 109–117.
- [33] I. Goodfellow, J. Pouget-Abadie, M. Mirza, B. Xu, D. Warde-Farley, S. Ozair, A. Courville, and Y. Bengio, "Generative adversarial nets," in *Advances in neural information processing systems*, 2014, pp. 2672–2680.